Pergamon

Int. J. Solids Structures Vol. 34, No. 8, pp. 949–967, 1997

0020–7683/97 $17.00 + .00

PII: S0020–7683(96)00064–9

FAILURE OF A THIN FILM DUE TO INCLUSIONS ON THE INTERFACE

PEI GU†, WEI YANG‡, C. F. SHIH§ and R. J. ASARO†

† Department of Applied Mechanics and Engineering Sciences, Mail Code 0411, University of California at San Diego, 9500 Cilman Drive, La Jolla, CA 92093-0411, U.S.A.

‡ Department of Engineering Mechanics, Tsinghua University, Beijing 100084, China

§ Division of Engineering, Brown University, Providence, RI 02912, U.S.A.

(*Received* 25 *October* 1995; *in revised form* 18 *April* 1996)

Abstract—This paper addresses failures near irregularities on the interface between a film and a substrate. Several boundary value problems, including two-dimensional and three-dimensional problems, involving inclusions of various shapes placed on the interface, are considered. The loading is induced by the lattice parameter mismatch between the film and substrate. Stresses near the interface and the inclusion boundary are of particular interest. The solutions show stress concentration around the inclusion boundary; in fact, a logarithmic singularity exists at the intersection of the inclusion, film and substrate. Emphasis is placed on identifying failures associated with high stresses near the inclusion. A theoretical prediction of the misfit strain to cause adhesion failure is obtained. The driving force for dislocation emission from the inclusion is calculated, and it is shown that dislocation emission from inclusions is favoured under a sufficiently large misfit strain. © 1997, Elsevier Science Ltd. All rights reserved.

1. INTRODUCTION

Thin films are widely used in electronic components and other advanced devices. Because high residual strains in the films due to either thermal expansion coefficient mismatch or lattice parameter mismatch between the films and substrates can cause device failures related to dislocation nucleation and interfacial cracking, the study of these mechanisms is a subject of interest. Many works addressing such problems can be found in the open literature. Examples of recent development include solutions to a large number of interfacial cracking problems by Hutchinson and Suo (1991), a detailed treatment for threading dislocations in the thin films by Freund (1993), and solutions to various stress-related problems in silicon technology, including film-edge induced stresses and dislocation generation in substrate due to these stresses, by Hu (1991).

The interfacial microstructure of a film/substrate system controls the performance of the system in more ways than one. It appears that this aspect has been overlooked by many. Recent experiments (Perovic *et al.*, 1989) have shown that β-SiC precipitates are formed on the interface between the Ge_xSi_{1-x} layer and Si substrate by molecular beam epitaxy, and dislocations emit from these precipitates when a critical particle size is reached. Also, it is possible that the surface of the substrate is not a perfect plane, i.e., there are irregularities on the substrate. Inclusions on the interface are sources of stress concentration, and therefore are the possible sites for failure initiation. Besides dislocation nucleation, adhesion failure occurs if stresses on the interface exceed its adhesion strength. In this paper, we examine the stress concentration near these inclusions, and attempt to identify failures resulting from these high stresses. For this purpose, an inclusion on the interface between a thin film and substrate is considered, and the loading arises from the lattice parameter mismatch between the film and substrate. In this study, we take the inclusion, film and substrate as elastically deforming bodies, i.e., the problem is solved by elasticity theory. The inclusion can be regarded as a local inhomogeneity. So, it is assumed that both the thickness of the film and the substrate are much larger than the size of the inclusion. Under these assumptions, we are able to obtain several analytical solutions for two-dimensional and three-dimensional inclusion problems.

The plan of this paper is as follows. In Section 2, the two-dimensional problem, an elliptical inclusion on the interface between a film and substrate, is analyzed. This idealized case admits an analytical solution with a relatively simple form which is obtained by complex variable method. In Section 3, the stresses on the interface between the film and substrate for the two-dimensional problem are examined. It is shown that high stresses are generated near the inclusion; in fact, the shear stress has a logarithmic singularity at the intersection of the inclusion, film and substrate. A theoretical prediction for the misfit strain to cause adhesion failure is obtained. Section 4 addresses the bending effect due to the misfit strain. The three-dimensional problem is solved in Section 5. Section 6 discusses dislocation emission from the inclusion, where the driving force for dislocation emission is derived, and it is shown that dislocation emission is favored for a sufficiently large misfit strain.

2. TWO-DIMENSIONAL PROBLEM: AN ELLIPTICAL INCLUSION

The mathematical problem shown in Fig. 1 is a film of thickness h bonded to the surface of a substrate. At the origin, there is an elliptical inclusion on the interface between the film and substrate. The major and minor axes are a and b, respectively. The film has a lattice parameter α_f, which differs from that of the substrate and inclusion, α_s. The inclusion and the substrate could have different lattice parameters, but this possibility is not considered here. The interface between film and substrate and the interface between film and inclusion are assumed to be coherent, so that a stress field is induced in the film, substrate and inclusion. Far away from the inclusion, its solution is known: the substrate is stress free and the film is subjected to biaxial uniform tension or compression

$$\sigma_0 = \frac{2\mu_1(1+\nu_1)}{1-\nu_1}\varepsilon_0, \tag{1}$$

where

$$\varepsilon_0 = \frac{\alpha_s - \alpha_f}{\alpha_f}. \tag{2}$$

Both the film and substrate have shear modulus μ_1 and Poisson's ratio ν_1, while these elastic constants for the inclusion are μ_2 and ν_2. For the semiconductor layered systems, the difference in elastic properties between the film and substrate is usually small; it is neglected here. As stated in the introduction, the film thickness is much larger than the inclusion size.

To solve the boundary value problem, one must match lattice parameters across the interfaces between the film and substrate and between the film and inclusion. On the interface between the film and substrate, there is a lattice parameter mismatch in the x and z directions (the z axis is perpendicular to the x and y axes shown in Fig. 1); but on the interface between the film and inclusion, there is a lattice parameter mismatch in all three directions, x, y and z. The solution to the three-dimensional problem can be obtained by considering two two-dimensional problems using an Eshelby-type superposition, as shown

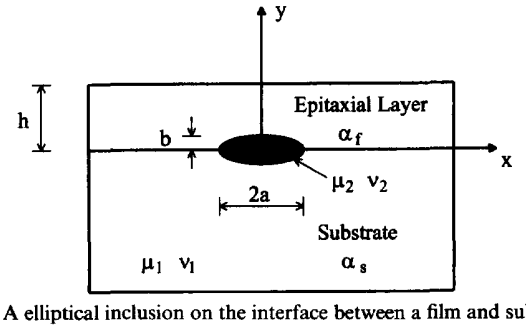

Fig. 1. A elliptical inclusion on the interface between a film and substrate.

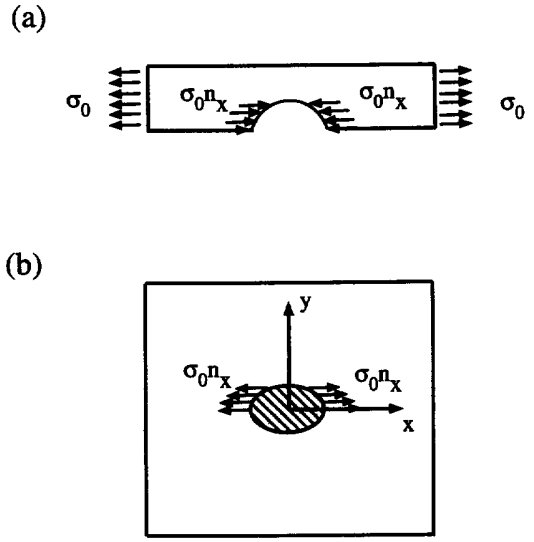

Fig. 2. A superposition scheme for solving lattice parameter mismatch problem.

in Fig. 2. First, we match the lattice parameters on both interfaces in the x and z directions, stretching the film by ε_0 in the x and z directions. The state of stress induced by this process is a uniform biaxial stress, $\sigma_{xx} = \sigma_{zz} = \sigma_0$. Next, a distribution of traction is applied to the interface between the film and inclusion so as to free it from stress, Fig. 2(b). In this cut and paste process, we have neglected the effect of Poisson's ratio. The stretch of the film induced a strain $\varepsilon_{yy} = -2\nu_1/(1-\nu_1)\varepsilon_0$; this strain reduces the lattice parameter in the y direction of the film. We have also neglected the difference in the lattice parameters in the y direction. These effects may be neglected if both the film and the substrate have the same lattice parameter in the y direction and the Poisson's ratio of the film is very small. We first solve the problem shown in Fig. 2(b), then the problem for the mismatch in the y direction.

The problem shown in Fig. 2(b) may be solved using the complex variable method (Muskhelishvili, 1953). Stress and displacement fields are generated by complex potentials $\phi(\xi)$ and $\psi(\xi)$ such that:

$$\begin{aligned} \sigma_{xx}+\sigma_{yy} &= 2[\phi'(\xi)+\overline{\phi'(\xi)}], \\ \sigma_{yy}-\sigma_{xx}+2i\sigma_{xy} &= 2[\bar{\xi}\phi''(\xi)+\psi'(\xi)], \\ 2\mu(u+iv) &= \kappa\phi(\xi)-\xi\overline{\phi'(\xi)}-\overline{\psi(\xi)}, \end{aligned} \tag{3}$$

where $\xi = x+iy$; $\kappa = 3-4\nu$ for plane strain; $\kappa = (3-\nu)/(1+\nu)$ for plane stress. The resultant force along the arc from $\xi = \xi_1$ to $\xi = \xi_2$ can be expressed as

$$F_x+iF_y = -i[\phi(\xi)+\xi\overline{\phi'(\xi)}+\overline{\psi(\xi)}]|_{\xi=\xi_1}^{\xi=\xi_2}. \tag{4}$$

The resultant force due to the traction acting on the inclusion boundary between $\xi = a$ and $\xi = \xi_0$ in Fig. 2(b) is

$$f(\xi_0) = \begin{cases} -i\dfrac{\mu_1(1+\nu_1)}{1-\nu_1}\varepsilon_0(\xi_0-\bar{\xi}_0) & \mathrm{Im}\xi_0 \geqslant 0 \\ 0 & \mathrm{Im}\xi_0 < 0. \end{cases} \tag{5}$$

Using a conformal mapping, $\xi = R(\zeta+m/\zeta)$ with $R = (a+b)/2$ and $m = (a-b)/(a+b)$, the elliptical inclusion is mapped onto a unit circle. Then, continuity conditions on the interface between the inclusion and matrix (the film and substrate) can be written as

$$\frac{1}{2\mu_1}\left[\kappa_1\phi_1(\tau)-\frac{\tau^2+m}{\tau(1-m\tau^2)}\overline{\phi_1'(\tau)}-\psi_1(\tau)\right]-\frac{1}{2\mu_2}\left[\kappa_2\phi_2(\tau)-\frac{\tau^2+m}{\tau(1-m\tau^2)}\overline{\phi_2'(\tau)}-\psi_2(\tau)\right]=0,$$

$$\left[\phi_1(\tau)+\frac{\tau^2+m}{\tau(1-m\tau^2)}\overline{\phi_1'(\tau)}+\psi_1(\tau)\right]-\left[\phi_2(\tau)+\frac{\tau^2+m}{\tau(1-m\tau^2)}\overline{\phi_2'(\tau)}+\psi_2(\tau)\right]=g(\tau), \quad (6)$$

where

$$g(\tau)=\begin{cases}-C\left(\tau-\dfrac{1}{\tau}\right) & \mathrm{Im}\tau\geqslant 0\\ 0 & \mathrm{Im}\tau<0,\end{cases}$$

$$C=\frac{\mu_1(1+\nu_1)}{1-\nu_1}\varepsilon_0 R(1-m), \quad (7)$$

and $|\tau|=1$. Here, $\phi_1(\zeta)$ and $\psi_1(\zeta)$ are complex potentials defined for the matrix, and $\phi_2(\zeta)$ and $\psi_2(\zeta)$ are complex potentials defined for the inclusion.

The solution to the problem is the four potentials which satisfy (6). Also, $\phi_1(\zeta)$ and $\psi_1(\zeta)$ have to give a stress free state at $z=\infty$. The detailed procedure to solve the problem is given in the Appendix, and the solution to the elliptical inclusion is obtained in terms of series. For a circular inclusion, the solution is a simple finite-term solution, which is given by

$$\phi_1(\zeta)=\frac{1}{\Gamma\kappa_1+1}\frac{C}{2\pi\mathrm{i}}\left[-2+\frac{\mathrm{i}\pi}{\zeta}+\frac{\zeta^2-1}{\zeta}\log\frac{\zeta+1}{\zeta-1}\right],$$

$$\psi_1(\zeta)=-\frac{\kappa_2}{\Gamma+\kappa_2}\frac{C}{2\pi\mathrm{i}}\left[-2+\frac{\mathrm{i}\pi}{\zeta}+\frac{\zeta^2-1}{\zeta}\log\frac{\zeta+1}{\zeta-1}\right]-\phi_1'(\zeta)\frac{1}{\zeta}+A\frac{1}{\zeta}, \quad (8)$$

where

$$A=\frac{\Gamma(1+\kappa_2)}{(\Gamma+\kappa_2)(2\Gamma+\kappa_2-1)}\frac{C}{2}, \quad (9)$$

and $\Gamma=\mu_2/\mu_1$. We shall not write here the expressions for $\phi_2(\zeta)$ and $\psi_2(\zeta)$ since the stress fields in the film and substrate are our interest.

The solution for the elliptical inclusion can be obtained directly in following special cases: $\Gamma=0$, $\Gamma=1$, and $\Gamma=\infty$. For $\Gamma=\infty$ (rigid inclusion), the solution is $\phi_1(\zeta)=\phi_2(\zeta)=\psi_1(\zeta)=\psi_2(\zeta)=0$. When $\Gamma=1$, the problem corresponds to a traction $\sigma_0\,\mathrm{d}y/\mathrm{d}s$ ($\mathrm{d}s$ is the differential arc length of the boundary of the ellipse) acting on the upper boundary of the ellipse in a homogeneous body. Its solution can be readily obtained by integrating a point force solution over the upper boundary of the inclusion. Similarly, for $\Gamma=0$, the solution can be obtained by integrating a point force acting on the upper boundary of the elliptical hole.

A step irregularity on the substrate surface shown in Fig. 3 gives rise to a similar problem. As before, both the film and substrate have the same elastic properties; there is no lattice parameter mismatch in the y direction, and the Poisson's ratio of the film is very small. The solution to the problem is obtained by the integration of a point force solution over $0<y<a$ with the point force being $\sigma_0\,\mathrm{d}y$. The two potentials are given by

$$\phi_1(\xi)=\frac{\sigma_0}{2\pi\mathrm{i}(1+\kappa)}[(\xi-\mathrm{i}a)\log(\xi-\mathrm{i}a)-\xi\log\xi],$$

$$\psi_1(\xi)=-\frac{\kappa\sigma_0}{2\pi\mathrm{i}(1+\kappa)}[(\xi-\mathrm{i}a)\log(\xi-\mathrm{i}a)-\xi\log\xi]+\frac{\sigma_0}{2\pi\mathrm{i}(1+\kappa)}\xi[\log(\xi-\mathrm{i}a)-\log\xi]. \quad (10)$$

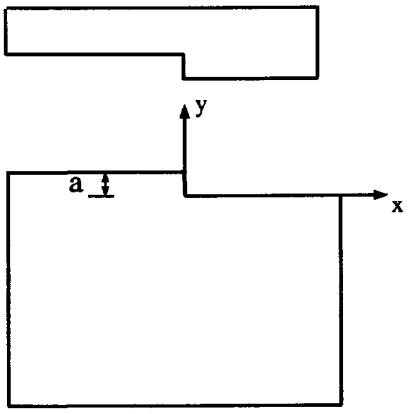

Fig. 3. A step irregularity.

We next solve the problem for the mismatch in the y direction. We view the problem as the one similar to Eshelby's internal problem, by assuming that there is a uniform eigenstrain in the upper half of the inclusion (the portion above the interface between the film and substrate) ε_{yy}^* due to the mismatch in the y direction. The eigenstrain is

$$\varepsilon_{yy}^* = \varepsilon_0\left(1+2\frac{\nu_1}{1-\nu_1}\right). \tag{11}$$

The term involving ν_1 represents the effect of the Poisson's ratio ν_1 in the cut and paste process discussed before, and the rest represents the effect of the difference in lattice parameters in the y direction. If there is no lattice parameter mismatch in the y direction,

$$\varepsilon_{yy}^* = 2\frac{\nu_1}{1-\nu_1}\varepsilon_0. \tag{12}$$

The mathematical problem can be formulated by the complex variable method, see List and Silberstein (1966). The continuity condition on the interface between the inclusion and the matrix is the same as (6), except in this case the right side of the first equation is $g(\tau)$ and that of the second equation is zero. Here,

$$g(\tau) = \begin{cases} \dfrac{\varepsilon_{yy}^*}{2}R(1-m)\left(\tau-\dfrac{1}{\tau}\right) & \mathrm{Im}\tau \geqslant 0 \\ 0 & \mathrm{Im}\tau < 0. \end{cases} \tag{13}$$

This shows that the problem can be solved in the similar way as that in the Appendix. The two potentials for a circular inclusion are given by

$$\phi_1(\zeta) = -\frac{\Gamma}{\Gamma\kappa_1+1}\frac{\mu_1\varepsilon_{yy}^*R}{2\pi\mathrm{i}}\left[-2+\frac{\mathrm{i}\pi}{\zeta}+\frac{\zeta^2-1}{\zeta}\log\frac{\zeta+1}{\zeta-1}\right],$$

$$\psi_1(\zeta) = -\frac{\Gamma}{\Gamma+\kappa_2}\frac{\mu_1\varepsilon_{yy}^*R}{2\pi\mathrm{i}}\left[-2+\frac{\mathrm{i}\pi}{\zeta}+\frac{\zeta^2-1}{\zeta}\log\frac{\zeta+1}{\zeta-1}\right]-\phi_1'(\zeta)\frac{1}{\zeta}+A_1\frac{1}{\zeta}, \tag{14}$$

where

$$A_1 = -\frac{\Gamma(1+\kappa_2)}{(\Gamma+\kappa_2)(2\Gamma+\kappa_2-1)}\frac{\mu_1\varepsilon_{yy}^*R}{2}. \tag{15}$$

Finally, we mention that the analysis for the mismatch in the y direction is the first order

approximation since we assume a uniform eigenstrain in the inclusion; in the real case the eigenstrain appears to be more complicated.

3. STRESSES ON THE INTERFACE BETWEEN THE FILM AND SUBSTRATE

Having the solution in Section 2, we examine the stresses on the interface between the film and substrate near an inclusion. For the most part of this section, we assume that the film and the substrate have the same lattice parameter in the y direction and the Poisson's ratio of the film is small, so that the solution for the problem shown in Fig. 2(b) is a valid solution. For a circular inclusion, the shear stress on the interface is

$$\sigma_{xy}(\rho,0) = -\frac{\sigma_0}{4\pi}\frac{1}{1+\Gamma\kappa_1}\left(-\frac{6}{\rho^3}+\frac{3-\rho^2}{\rho^4}\log\frac{\rho+1}{\rho-1}\right) + \frac{\sigma_0}{4\pi}\frac{\kappa_2}{\Gamma+\kappa_2}\left(-\frac{2}{\rho}+\frac{1+\rho^2}{\rho^2}\log\frac{\rho+1}{\rho-1}\right), \quad (16)$$

where $\rho = x/a$, and is either greater than 1 or less than -1. It has a logarithmic singularity at the intersection of the film, substrate and inclusion, $\rho = \pm 1$. The singular term is

$$\sigma_{xy}(\rho,0) = \frac{\sigma_0}{2\pi}\left(\frac{\kappa_2}{\Gamma+\kappa_2}-\frac{1}{1+\Gamma\kappa_1}\right)\log\frac{\rho+1}{\rho-1} \quad (17)$$

as $\rho \to \pm 1$. The expression before the logarithmic function in the above expression is a logarithmic stress intensity factor, which varies with Γ, κ_1 and κ_2. For fixed $\kappa_1 = \kappa_2 = 2.6$ (plane strain with $\nu_1 = \nu_2 = 0.1$), the logarithmic stress intensity factor is the largest when $\Gamma = 1$, and it vanishes when $\Gamma = 0$ (hole) and $\Gamma = \infty$ (rigid inclusion). The singularity is so weak that its zone of dominance is very small. This can be seen from Fig. 4, where (16) is plotted for several Γ's. In this figure, the shear stress for $\Gamma = 0$ is larger than the shear stress for $\Gamma = 1$ except the very small portion near $\rho = 1$. Also, the shear stress decreases quickly to zero, and its effective zone is about 3–4 times the size of the inclusion.

To examine the geometrical influence of the inclusion, the shear stress caused by an elliptical inclusion is plotted in Fig. 5 for several values of b/a, where we choose $\Gamma = 1$ and $\kappa_1 = \kappa_2 = 2.6$ (plane strain with $\nu_1 = \nu_2 = 0.1$). It shows that σ_{xy} increases as b/a increases. This is because the mismatch increases as b/a increases. Also, the shear stress decays more quickly for smaller b/a.

An inclusion on the interface between the film and substrate can generate high shear stress. When the inclusion and matrix have the same elastic properties, $\Gamma = 1$ and $\kappa_1 = \kappa_2 = 2.6$ (plane strain with $\nu_1 = \nu_2 = 0.1$), the shear stress at a distance $0.1a$ ahead of

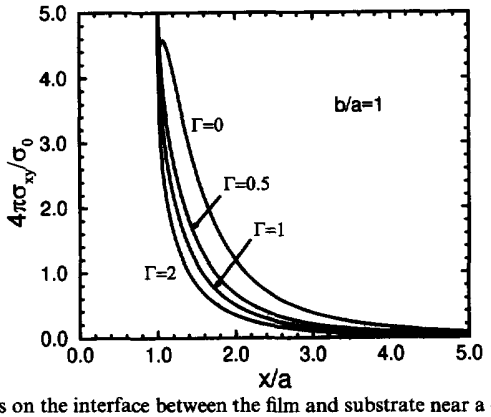

Fig. 4. Shear stress on the interface between the film and substrate near a circular inclusion.

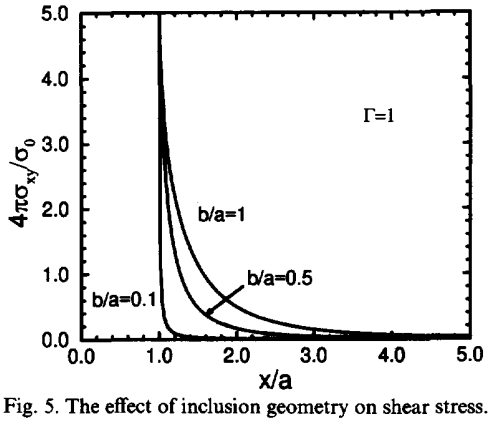

Fig. 5. The effect of inclusion geometry on shear stress.

the inclusion (the shear stress is singular at the intersection of the film, substrate and inclusion) is

$$\sigma_{xy} = 0.23\sigma_0 \tag{18}$$

for a circular inclusion. Consider growing a GaAs film on Si substrate, and neglect the difference in elastic properties between GaAs and Si. For these materials, $\varepsilon_0 = -0.04$ and $E_{GaAs} = 85$ GPa. Then, (18) gives $\sigma_{xy} = -0.9$ GPa.

Near a circular inclusion, the normal stress on the interface between the film and substrate is

$$\sigma_{yy}(\rho, 0) = \frac{\sigma_0}{4}\frac{\kappa_2 - 1}{2\Gamma + \kappa_2 - 1}\frac{1}{\rho^2} - \frac{3\sigma_0}{4}\frac{1}{1+\Gamma\kappa_1}\frac{1}{\rho^4}, \tag{19}$$

where $\rho = x/a$, and is either greater than 1 or less than -1. We note that it does not have a singularity as does σ_{xy}. For $\Gamma = 1$ and $\kappa_1 = \kappa_2 = 2.6$ (plane strain with $\nu_1 = \nu_2 = 0.1$), the maximum normal stress which occurs at $\rho = \pm 1$ is

$$\sigma_{yy} = -0.1\sigma_0. \tag{20}$$

If $\varepsilon_0 < 0$, the normal stress is a peeling stress. The above expression shows that a large compressive residual strain gives a large peeling stress on the interface, which is a driving force for adhesion failure of the interface. If $\varepsilon_0 > 0$, it is a compressive stress. For the GaAs/Si example, the maximum peeling stress is 0.4 GPa. Figure 6 shows σ_{yy} vs ρ for several values of Γ.

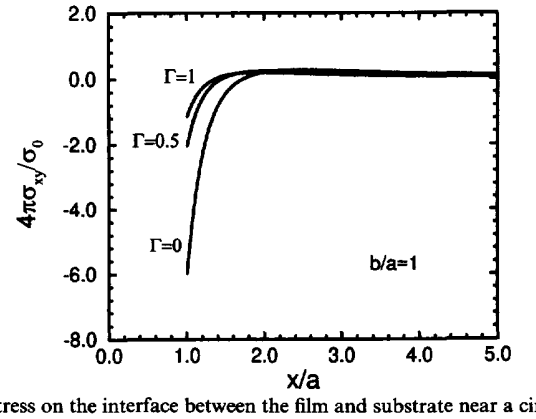

Fig. 6. Normal stress on the interface between the film and substrate near a circular inclusion.

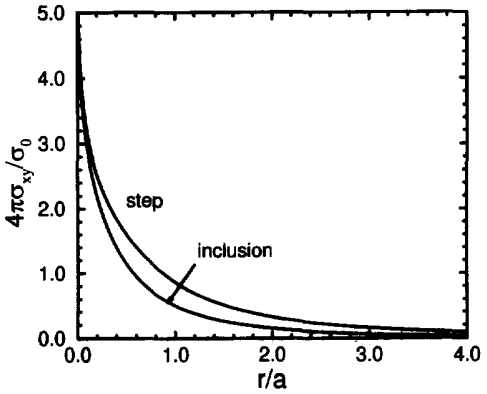

Fig. 7. Comparison of shear stresses near a circular inclusion and near a step irregularity, on the interface between the film and substrate.

Near a step irregularity, the shear stress on the interface between the film and substrate is

$$\sigma_{xy}(\rho, 0) = \frac{\sigma_0}{\pi(1+\kappa)}\left[\frac{1}{\rho^2+1} - \frac{1-\kappa}{4}\log\left(1+\frac{1}{\rho^2}\right)\right], \tag{21}$$

where $\rho = x/a$, and $\rho > 0$. The shear stresses on the interface near a step irregularity and near a circular inclusion are compared in Fig. 7. As expected, it shows that the step irregularity produces larger shear stress on the interface.

If there are no inclusions and step irregularities on the interface, there are no stresses acting on the interface. Therefore, adhesion failure may not occur. If the residual strain ε_0 in the thin film causes adhesion failure due to inclusions or step irregularities, we estimate it from above solutions. Suppose that the interfacial adhesion strength, i.e., the summation of all atomic bonding forces between the adjoining material surfaces for an ideal planar interface, is known, and let the critical normal stress be σ_b and the critical shear stress be τ_b. Then, from (18) and (20), the mismatch stress σ_0 to cause adhesion failure is given by the smaller of

$$\begin{aligned} |\sigma_0| &= 4.35\tau_b, \\ |\sigma_0| &= 10\sigma_b, \end{aligned} \tag{22}$$

for compressive σ_0. For tensile σ_0, this prediction is

$$\sigma_0 = 4.35\tau_b. \tag{23}$$

In writing (22) and (23), we have assumed that adhesion failure caused by shear occurs at a distance $0.1a$ ahead of the inclusion. Besides calculating atomic bonding forces, the interface adhesion strength can be measured by a number of methods which have been discussed in Alexopoulos and O'Sullivan (1990). Due to the difficulty in handling these tests, the data obtained by these methods are usually considered to be qualitative in nature.

It is seen that either a large residual strain or poor interface bonding could lead to adhesion failure. In the GaAs/Si example discussed above, the film is subjected to compressive residual stress and the normal stress on the interface is a peeling stress. If we assume that the failure mode is the adhesion failure by the peeling stress, the criterion predicts that the adhesion failure occurs if σ_b is less than 0.4 GPa. The development of the initial failure could lead to large scale fracture, such as film buckling. The mechanics of film buckling has been studied by Evans and Hutchinson (1984), and the cracking and buckling processes of a film/substrate system have been characterized in terms of the behavior of the film and substrate, and the interface bonding by Evans *et al.* (1988).

The effect of the mismatch in the y direction can be estimated using the solution for a circular inclusion given by (14) and (15). The shear stress on the interface between the film and substrate near the inclusion is

$$\sigma_{xy}(\rho,0) = \frac{\mu_1 \varepsilon_{yy}^*}{2\pi}\frac{\Gamma}{1+\Gamma\kappa_1}\left(-\frac{6}{\rho^3}+\frac{3-\rho^2}{\rho^4}\log\frac{\rho+1}{\rho-1}\right) + \frac{\mu_1\varepsilon_{yy}^*}{2\pi}\frac{\Gamma}{\Gamma+\kappa_2}\left(-\frac{2}{\rho}+\frac{1+\rho^2}{\rho^2}\log\frac{\rho+1}{\rho-1}\right), \quad (24)$$

where $\rho = x/a$, and is either greater than 1 or less than -1; the normal stress is

$$\sigma_{yy}(\rho,0) = \mu_1\varepsilon_{yy}^*\frac{\Gamma}{2\Gamma+\kappa_2-1}\frac{1}{\rho^2}+\frac{3\mu_1\varepsilon_{yy}^*}{2}\frac{\Gamma}{1+\Gamma\kappa_1}\frac{1}{\rho^4}. \quad (25)$$

We examine the effect of the Poisson's ratio using (12) for ε_{yy}^*. Since the stresses are proportional to the Poisson's ratio ν_1, they can be neglected if the Poisson's ratio is small. The larger the Poisson's ratio, the larger its effect on the stress field. Few numerical examples for the stresses are given below when ν_1 is small, by taking $\Gamma = 1$ and $\kappa_1 = \kappa_2$. At $\rho = 1$, the normal stress is 0.006 σ_0 for $\nu_1 = 0.01$, and 0.06 σ_0 for $\nu_1 = 0.1$. At $\rho = 1.1$, the shear stress is 0.001 σ_0 for $\nu_1 = 0.01$, and 0.01 σ_0 for $\nu_1 = 0.1$. It appears that the normal stress is larger than the shear stress for the mismatch in the y direction.

4. BENDING EFFECT

If the film and substrate have finite thicknesses, the solution described in the preceding sections must be corrected. Four self-equilibrating bending moments are applied to the film and substrate, and two of them in the x-y plane are shown in Fig. 8. We assume the thickness of the substrate h_s is much larger than that of the film h, and the thickness of the film is much larger than the size of the inclusion $R = (a+b)/2$. The magnitude of these bending moments depends on the thicknesses of film and substrate, and is given by

$$M = \tfrac{1}{2}hh_s\sigma_0. \quad (26)$$

These bending moments act at a distance $h_s/2$ from the bottom of the substrate. For $\Gamma = 1$ and $\kappa_1 = \kappa_2$, M does not cause shear and normal stresses at the interface between the film and substrate, and the stress and strain fields in the film and substrate are given by beam theory. For $\Gamma \neq 1$, the bending moments induce stresses at the interface, which we calculate as follows.

Note that the two moments in the x direction do not cause stresses on the interface if the inclusion and the matrix have the same curvature in the y-z plane (the z axis is perpendicular to the x and y axes shown in Fig. 1). Consequently, it is only necessary to consider the deformation caused by the two moments shown in Fig. 8. If we use the displacement field of a homogeneous problem ($\Gamma = 1, \kappa_1 = \kappa_2$) as a solution to the inhomogeneous problem there is a traction jump on the inclusion boundary. The solution may be

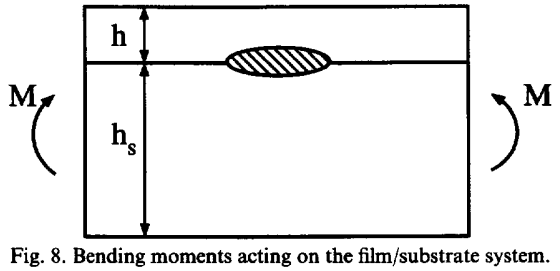

Fig. 8. Bending moments acting on the film/substrate system.

corrected by superposing an equal and opposite traction jump on the inclusion boundary. The traction jump, expressed as a resultant force on the inclusion boundary, is

$$g(\tau) = ic_1\tau^2 + ic_1\frac{1}{\tau^2} - 2ic_1 + c_2\tau - c_2\frac{1}{\tau},$$

$$c_1 = \frac{1}{8}R^2(1-m)^2(1-\Gamma)\frac{M}{I},$$

$$c_2 = -\frac{1}{2}R(1-m)(1-\Gamma)\frac{Mh_s}{2I}, \tag{27}$$

where $I = (h_s+h)^3/12$. For simplicity, we have taken $\kappa_1 = \kappa_2$ to derive (27). When $h_s \to \infty$, $g(\tau) = 0$, which states the fact that a substrate with infinite thickness does not induce bending curvature. The function $g(\tau)$ plays the same role as that in Section 2, so that the solution can be obtained by the same way as that in the Appendix. For a circular inclusion, the solution is

$$\phi_1(\zeta) = \frac{1}{\Gamma\kappa+1}\left(ic_1\frac{1}{\zeta^2} - c_2\frac{1}{\zeta}\right),$$

$$\psi_1(\zeta) = -\frac{\kappa}{\Gamma+\kappa}ic_1\frac{1}{\zeta^2} - \frac{1-\kappa}{2\Gamma+\kappa-1}c_2\frac{1}{\zeta} - \frac{1}{\zeta}\phi_1'(\zeta), \tag{28}$$

where $\kappa = \kappa_1 = \kappa_2$. Then, the normal and shear stresses on the interface between the film and substrate near the inclusion are

$$\sigma_{xy}(\rho,0) = \frac{3Rh}{4h_s^2}\sigma_0(1-\Gamma)\left(\frac{1}{\Gamma\kappa+1}\frac{6\rho^2-8}{\rho^5} + \frac{\kappa}{\Gamma+\kappa}\frac{2}{\rho^3}\right),$$

$$\sigma_{yy}(\rho,0) = -\frac{3h}{2h_s}\sigma_0(1-\Gamma)\left(\frac{1}{\Gamma\kappa+1}\frac{3}{\rho^4} + \frac{1-\kappa}{2\Gamma+\kappa-1}\frac{1}{\rho^2}\right). \tag{29}$$

The condition, h, $h_s \gg R$, must be satisfied for the solution to be valid as explained at the beginning of the section. The normal stress is in compression for a soft inclusion ($\Gamma < 1$), and the shear stress is proportional to a coefficient in (29), i.e.,

$$\sigma_{xy}(\rho,0) \sim \frac{3Rh}{4h_s^2}\sigma_0. \tag{30}$$

Suppose that

$$h_s > 10h > 1000R, \tag{31}$$

we have from (30) that

$$\sigma_{xy}(\rho,0) \sim \frac{9}{80000}\sigma_0. \tag{32}$$

The shear stress may be neglected.

5. THREE-DIMENSIONAL PROBLEM

In general, the problem of an inclusion on the interface between the film and substrate is likely to be a three-dimensional problem. The analytical solution to a three-dimensional

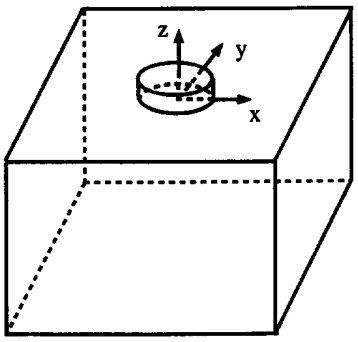

Fig. 9. Three-dimensional problem.

inclusion problem is difficult and available solutions can be found in Mura (1987). In this section, by assuming that the elastic properties of the inclusion, film and substrate are the same, we find an exact solution to the three-dimensional inclusion problem for the case that the loading is lattice parameter mismatch between the film and substrate. As before, we assume that the film thickness is much larger than the size of the inclusion.

The three-dimensional problem can be decomposed into two problems. One represents the lattice parameter mismatch in the x and y directions, and the other represents the mismatch in the z direction (the x, y, z axes are shown in Fig. 9, and the film thickness direction is designated as z). As in Section 2, we shall assume that there is no lattice parameter mismatch in the z direction and the Poisson's ratio of the film is very small. In other words, the mismatch in the z direction can be neglected. Following the argument given in Section 2, the solution to the three-dimensional problem can be obtained by integrating a point force solution over the inclusion boundary. To do this, we write the solution of a point force in the following form

$$\sigma_{ij}^{k}(x,y,z) = \frac{P^{k}}{8\pi(1-\nu)}\hat{\sigma}_{ij}^{k}(x-x_0, y-y_0, z-z_0), \tag{33}$$

where indices i, j and k vary from 1 to 3, designating the x, y and z in turn; P^k is a vector force in the k direction. The function $\hat{\sigma}_{xy}^{k}$ has the dimension 1/[length]^2. Equation (33) represents the stress field due to a point force in the direction k acting at (x_0, y_0, z_0). The stresses induced by an inclusion or a step irregularity can be written as

$$\sigma_{ij}(x,y,z) = \frac{\sigma_0}{8\pi(1-\nu)}\left[\int_{(x_0,y_0,z_0)\in S} n_x\hat{\sigma}_{ij}^{1}(x-x_0, y-y_0, z-z_0)\,\mathrm{d}S + \int_{(x_0,y_0,z_0)\in S} n_y\hat{\sigma}_{ij}^{2}(x-x_0, y-y_0, z-z_0)\,\mathrm{d}S\right], \tag{34}$$

where S is the inclusion boundary that is surrounded by the film, or the vertical part of the step irregularity, and $\mathbf{n} = (n_x, n_y, n_z)$ is the unit outward normal to the inclusion boundary at (x_0, y_0, z_0). For the two normal stresses parallel to the interface between the film and substrate, σ_{xx} and σ_{yy}, the residual stress σ_0 has to be added to obtain the total stresses. The two surface integrals in (34) can not be evaluated analytically for an arbitrary inclusion shape. They cannot even be evaluated exactly for some simple shapes like a sphere. However, the surface integrals can be reduced to line integrals to simplify them in many cases. Two examples will be given below.

The first example is a corner step irregularity, as shown in Fig. 10. The corner step irregularity occupies the region, $x \leqslant 0$, $y \leqslant 0$ and $0 \leqslant z \leqslant a$. Note that, if we extend the above step irregularity region in the y direction and let it occupy $x \leqslant 0$, $-\infty \leqslant y \leqslant \infty$ and $0 \leqslant z \leqslant a$, it becomes the two-dimensional problem which was solved in Section 2. The purpose of this example is to examine the effect of a corner on the stress distribution. In

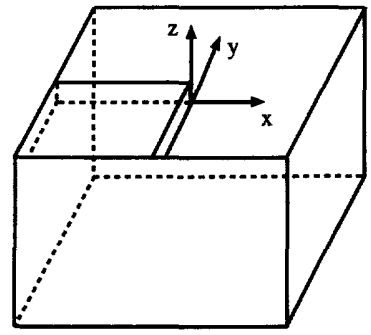

Fig. 10. A corner step irregularity.

this case, the integrations in (34) can be evaluated analytically. The two shear stresses on the plane $z = 0$ are given by

$$\sigma_{xz}(x,y,0) = \frac{\sigma_0}{8\pi(1-\nu)}\left[-\frac{a^2 y}{(x^2+a^2)\sqrt{x^2+y^2+a^2}} + \frac{a^2}{x^2+a^2} + (1-2\nu)\log\frac{y+\sqrt{x^2+y^2+a^2}}{y+\sqrt{x^2+y^2}}\right],$$

$$\sigma_{yz}(x,y,0) = \frac{\sigma_0}{8\pi(1-\nu)}\left[-\frac{a^2 x}{(y^2+a^2)\sqrt{x^2+y^2+a^2}} + \frac{a^2}{y^2+a^2} + (1-2\nu)\log\frac{x+\sqrt{x^2+y^2+a^2}}{x+\sqrt{x^2+y^2}}\right]. \tag{35}$$

The shear stress σ_{xz} in (35) has a logarithmic singularity on the straight line, $x = 0$ and $y \leqslant 0$, as in the two-dimensional case. The corner introduces a stress σ_{yz}, which is zero in the two-dimensional case. Far away from the corner, its influence vanishes so that σ_{yz} approaches zero as $y \to \pm\infty$. A plot of σ_{yz} vs y when $x = 0.01a$ is given in Fig. 11. We observe that the σ_{yz} is negligible for $|x| > 5a$. On the other hand, σ_{xz} approaches the two-dimensional solution given in Section 2 as $y \to -\infty$, and vanishes when $y \to +\infty$. The variation of σ_{xz} along the y axis when $x = 0.01a$ is also shown in Fig. 11. The two shear stresses at $y = 0$, $z = 0$ are given by

$$\sigma_{xz}(x,0,0) = \frac{\sigma_0}{8\pi(1-\nu)}\left(\frac{a^2}{x^2+a^2} + (1-2\nu)\log\sqrt{\frac{x^2+a^2}{x^2}}\right),$$

$$\sigma_{yz}(x,0,0) = \frac{\sigma_0}{8\pi(1-\nu)}\left(\frac{a^2}{\sqrt{x^2+a^2}(x+\sqrt{x^2+a^2})}\right)$$

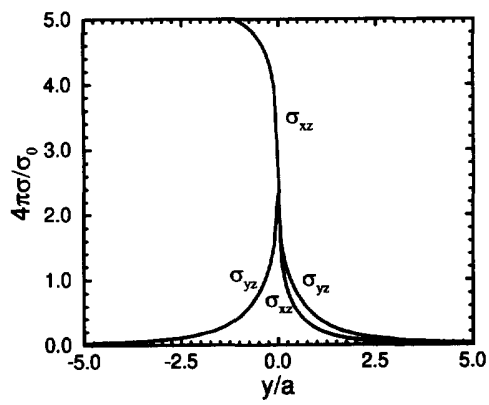

Fig. 11. Shear stresses near a corner step irregularity.

$$+(1-2\nu)\log\frac{x+\sqrt{x^2+a^2}}{2x}\Bigg) \tag{36}$$

for $x > 0$. Comparing $\sigma_{xz}(x,0,0)$ with $\sigma_{xz}(x,-\infty,0)$, we see that there is a simple relationship between them,

$$\sigma_{xz}(x,-\infty,0) = 2\sigma_{xz}(x,0,0). \tag{37}$$

This tells us that by traveling from $y = -\infty$ to $y = 0$, σ_{xz} reduces to half of its value at $y = -\infty$, and σ_{yz} rises from zero to the one given in (36). Also, we have another relationship,

$$\sigma_{xz}^2(x,0,0)+\sigma_{yz}^2(x,0,0) < \sigma_{xz}^2(x,-\infty,0) \tag{38}$$

for $x > 0$. This says that on the interface between the film and substrate the total shear stress at $(x,0,0)$ is less than the total shear stress at $(x,-\infty,0)$, because the corner relieves stress concentration.

The second example is a circular plate above the interface of the film and substrate, as shown in Fig. 9. Both the thickness and radius of the circular plate are a. The axisymmetry of the problem renders σ_{rz} (r, θ and z are used instead of x, y and z) is the only nontrial shear stress, which on the interface is given by

$$\begin{aligned}\sigma_{rz}(r,0,0) = &-\frac{\sigma_0 a}{4\pi(1-\nu)}\int_0^{\pi}(r-a\cos\theta)(r\cos\theta-a)\\ &\times\left[\frac{1}{(r^2-2ar\cos\theta+2a^2)^{3/2}}-\frac{1}{(r^2-2ar\cos\theta+a^2)^{3/2}}\right]d\theta\\ &-\frac{\sigma_0 a}{4\pi(1-\nu)}(1-2\nu)\int_0^{\pi}\cos\theta\left[\frac{1}{(r^2-2ar\cos\theta+2a^2)^{1/2}}\right.\\ &\left.-\frac{1}{(r^2-2ar\cos\theta+a^2)^{1/2}}\right]d\theta,\end{aligned} \tag{39}$$

after evaluating the integrals in (34) along the z direction. Further derivation shows that the line integrals in above expression can be written in terms of elliptical integrals. The σ_{rz} has a logarithmic singularity at $r = a$, and a plot of σ_{rz} vs r is shown in Fig. 12.

We can also give the expressions for other stress components in the above two examples by evaluating the integrals in (34). The inclusion shape has a strong effect on the stresses near the inclusion. For the circular plate, $\sigma_{rz}(1.1a,0,0) = 0.186\sigma_0$ and σ_{zz}

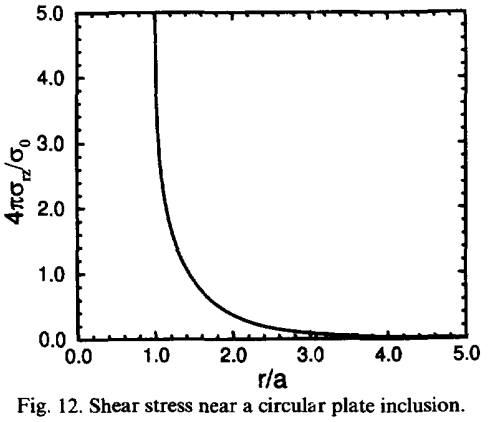

Fig. 12. Shear stress near a circular plate inclusion.

$(a, 0, 0) = -0.02\sigma_0$, whereas for the two-dimensional circular inclusion in Section 2, the two stresses on the interface between the film and substrate are $0.23\sigma_0$ and $-0.1\sigma_0$, respectively.

6. DISLOCATIONS IN THIN FILMS

Over the past few decades, the so-called threading dislocations which form in epitaxial layers used for semiconductor materials have received attention. Threading dislocations occur when the thickness of an epitaxial layer reaches a critical value. The critical thickness has been treated by a number of authors, including Matthews and Blakeslee (1974), People and Bean (1985) and Freund (1990). But the mechanism responsible for forming such dislocations has not yet been fully understood. Eaglesham *et al.* (1989) have discussed the diamond defect as a source for dislocation nucleation. Dodson (1988) has argued that the stress concentration around clusters of impurity atoms is a good source to generate dislocations. The experiments by Perovic *et al.* (1989) have shown that, for films grown by molecular beam epitaxy, there are precipitates on the interface between the film and substrate, and V-shaped threading dislocations are emitted from the heterogeneous particles if their size exceeds critical value, while particles below the critical size are coherent with surrounding matrix. Among the two types of heterogeneous precipitates on the interface, it was found that β-SiC precipitates tend to generate dislocations, whereas SiO_x precipitates are dislocation-free (Hull, 1986) because they are in an amorphous state which eliminates misfit strains. In this section, we consider these observations in the light of our solutions to the state of stresses near inclusions in strained layer systems.

We examine the shear stress, which provides the glide force for dislocation motion, on possible slip planes around the inclusion. Two representatives of the slip planes shown in Fig. 13 are chosen for the two-dimensional problems (circular inclusion and step irregularity) whose solutions have been obtained in Section 2. The orientation of these slip planes is chosen here to form the angle, $\theta = \sin^{-1}(1/\sqrt{3})$, with the interface between the film and substrate. We neglect the difference in elastic properties among the inclusion, film and substrate. Figure 14 shows the shear stress for the circular inclusion, where r/a is the distance from the inclusion; it has the same trend for the step irregularity. The shear stress at the inclusion boundary on slip plane #1 for the step irregularity has a logarithmic singularity, and for the circular inclusion it is nearly twice as large as that far away from the inclusion, the homogeneous solution. The high shear stress state provides a good condition to generate dislocations. The shear stress on slip plane #2 is somewhat different from slip plane #1. Although there is a logarithmic singularity at the inclusion boundary, the shear stress changes sign at a distance very close to the inclusion, and increases to the homogeneous solution as the distance increases. The shear stress near the inclusion on any

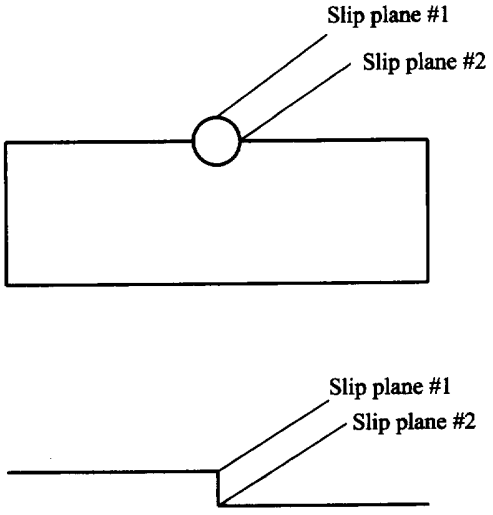

Fig. 13. Two possible slip planes which intersect the circular inclusion and the step irregularity.

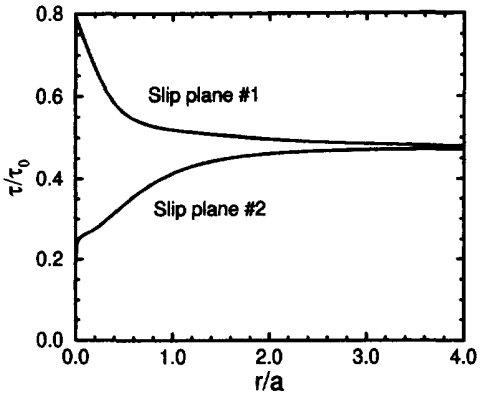

Fig. 14. Shear stress near the circular inclusion on the two slip planes shown in Fig. 13.

slip plane, which is between slip planes #1 and #2 and is parallel to these two slip planes, is less than that on slip plane #1.

If the inclusion is admitted as a source for dislocation nucleation in a thin film, the driving force for the emitted dislocation can be derived as follows. The energy dissipation associated with the dislocation motion is expressed as

$$W(S) = -\frac{1}{2}\int_S \sigma_{ij}^D n_j b_i \, ds - \int_S \sigma_{ij}^A n_j b_i \, ds, \tag{40}$$

where S is the glide plane; n_j is the outward normal of the left portion of the film divided by the slip plan; the Burgers vector b_i is the displacement of the left side of the glide plane minus that of the right side of the glide plan. In the expression, the stress field σ_{ij}^D is due to the dislocation, and σ_{ij}^A is due to the applied load, namely the lattice parameter mismatch. Define the driving force G from the time rate of the energy dissipation as

$$\dot{W}(S) = Gv, \tag{41}$$

where v the speed of the emitted dislocation. The driving force is derived in the same way as that in Freund (1990) for threading dislocation, and is given by

$$G = -\tfrac{1}{2}\sigma_{ij}^D(A) n_j b_i - \sigma_{ij}^A(B) n_j b_i, \tag{42}$$

where $\sigma_{ij}^D(A)$ and $\sigma_{ij}^A(B)$ denote the corresponding stresses at the inclusion boundary and the position of the emitted dislocation, respectively. Note that since the difference in elastic properties between the inclusion and the matrix is neglected, there is no image force due to the mismatch of elastic properties acting on the dislocation. The first term in (42) can be calculated from the solution of a dislocation in a infinite body, and the second term can be calculated from the solution obtained in Section 2. We finally obtain

$$\frac{G}{\mu b} = -\frac{1}{4\pi(1-\nu)}\frac{b}{a}\left(\frac{r}{a}\right)^{-1} + \frac{2(1+\nu)}{1-\nu}\varepsilon_0 T\left(\frac{r}{a}\right), \tag{43}$$

where r is the distance between the dislocation and the inclusion boundary, a is the size of the inclusion, b is the magnitude of the Burgers vector, and $T(r/a)$ is a nondimensional function obtained from the stresses $\sigma_{ij}^A(B)$. Given the inclusion size, the magnitude of the Burgers vector and the misfit strain, the distance from the inclusion at which $G = 0$ (equilibrium point), namely r^*, is determined from (43). For $r > r^*$, $G > 0$; for $r < r^*$, $G < 0$. If the dislocation is formed at the distance less than r^* from the inclusion, it will be driven back to the inclusion boundary; otherwise, it will be emitted. We take the circular inclusion as an example, and consider slip plane #1. For $b = 0.4$ nm and $\varepsilon_0 = 0.04$,

$r^* = 0.458$ nm if $a = 100$ nm; $r^* = 0.473$ nm if $a = 10$ nm; $r^* = 0.673$ nm if $a = 1$ nm. When ε_0 is increased to 0.06, r^* is 0.305 nm, 0.311 nm and 0.415 nm for the above three cases, respectively. The larger the misfit strain and the inclusion size, the smaller the critical distance r^*. When r^* is less than the core cut-off radius, we have the case that the dislocation formed at the inclusion boundary is emitted spontaneously (see Rice and Thomson (1974) for dislocation emission from a crack tip). The numerical results here show that dislocation emission is favored for large misfit strain. For inclusions in shapes other than the two we have treated here, the driving force may be obtained in the same manner. Zhang and Yang (1994) have studied the process of dislocation emission from a spherical cavity on the interface between the film and substrate.

7. CONCLUDING REMARKS

Solutions are presented for several boundary value problems involving various shaped inclusions located on the interface between a thin film and a substrate. The film and the substrate have different lattice parameters. The solutions exhibit stress concentrations around the inclusions. There is a logarithmic stress singularity at the intersection of the film, substrate and inclusion. Moreover, the shear stress around the inclusion can be nearly twice as large as the remote field given by the homogeneous solution. High stresses around inclusions and on the interface between film and substrate could cause dislocation nucleation and adhesion failure. A theoretical prediction of the misfit strain to cause adhesion failure is obtained. The driving force for dislocation emission from the inclusion is calculated, and it is shown that dislocation emission from inclusions is favored for sufficiently large misfit strain. The results suggest that small inclusions (compared to film thickness) on the interface between a film and a substrate can be the sources for failure initiation in the layered system. These failures can be precursors to failures on a larger scale: adhesion failure can lead to film buckling; and dislocation emission eventually causes threading dislocations as shown by Zhang and Yang (1994) for a spherical cavity.

Acknowledgements—PG and CFS acknowledge the support from the Office of Naval Research through Grant N00014-90-J-1380. PG and RJA acknowledge the support from the Office of Naval Research through Grant N00014-93-1-1164.

REFERENCES

Alexopoulos, P. S. and O'Sullivan, T. C. (1990) Mechanical properties of thin films. *A. Rev. Mat. Sci.* **20,** 391–420.

Dodson, B. W. (1988) Nature of misfit dislocation sources in strained-layer semiconductor structures. *Appl. Phys. Lett.* **53,** 394–396.

Eaglesham, D. J., Kvam, E. P., Maher, D. M., Humphreys, C. J. and Bean, J. C. (1989) Dislocation nucleation near the critical thickness in GeSi/Si strained layers. *Phil. Mag.* **A59,** 1059–1073.

Evans, A. G. and Hutchinson, J. W. (1984) On the mechanics of delamination and spalling in compressed films. *Int. J. Solids Structures* **20,** 455–466.

Evans, A. G., Drory, M. D. and Hu, M. S. (1988) The cracking and decohesion of thin films. *J. Mater. Res.* **3,** 1043–1049.

Freund, L. B. (1990) The driving force for glide of a threading dislocation in a strained epitaxial layer on a substrate. *J. Mech. Phys. Solids* **38,** 657–679.

Freund, L. B. (1993) The mechanics of dislocations in strained-layer semiconductor materials. *Adv. Appl. Mech.* **30,** 1–66.

Hu, S. M. (1991) Stress-related problems in silicon technology. *J. Appl. Phys.* **70,** R53–R80.

Hull, R., Bean, J. C., Gibson, J. M., Joy, D. C. and Twigg, M. E. (1986) Trapping of oxygen at homoepitaxial Si–Si interfaces. *Appl. Phys. Lett.* **49,** 1287–1289.

Hutchinson, J. W. and Suo, Z. (1991) Mixed mode cracking in layered materials. *Adv. Appl. Mech.* **29,** 63–191.

List, R. D. and Silberstein, J. P. O. (1966) Two-dimensional elastic inclusion problems. *Proc. Cambridge Phil. Soc.* Vol. 62, pp. 303–311.

Matthews, J. W. and Blakeslee, A. E. (1974) Defects in epitaxial multilayers. *J. Crystal Growth* **27,** 118–125.

Mura, T. (1987) *Micromechanics of Defects in Solids*, 2nd edn. Martinus Nijhoff Publishers.

Muskhelishivili, N. I. (1953) *Some Basic Problems of the Mathematical Theory of Elasticity*, 3rd edn, Noordhoff.

People, R. and Bean, J. C. (1985) Calculation of critical layer thickness versus lattice mismatch for Ge_xSi_{1-x}/Si strained-layer heterostructures. *Appl. Phys. Lett.* **47,** 322–324.

Perovic, D. D., Weatherly, G. C., Baribeau, J.-M. and Houghton, D. C. (1989) Heterogeneous nucleation sources in molecular beam epitaxy-grown Ge_xSi_{1-x}/Si strained layer superlattices. *Thin Solid Films.* **183,** 141–156.

Rice, J. R. and Thomson, R. (1974) Ductile versus brittle behaviour of crystals. *Phil. Mag.* **29,** 73–97.

Zhang, H. and Yang, W. (1994) Three-dimensional dislocation loops generated from a weak inclusion in a strained material heterostructure. *J. Mech. Phys. Solids* **42**, 913–930.

APPENDIX

After the conformal mapping, the two potentials for the matrix, $\phi_1(\zeta)$ and $\psi_1(\zeta)$, are analytical outside the unit circle $|\zeta| = 1$, and admit the forms,

$$\phi_1(\zeta) = \frac{a_1}{\zeta} + \frac{a_2}{\zeta^2} + \cdots,$$

$$\psi_1(\zeta) = \frac{b_1}{\zeta} + \frac{b_2}{\zeta^2} + \cdots. \tag{A.1}$$

The two potentials for the inclusion, $\phi_2(\zeta)$ and $\psi_2(\zeta)$, are not analytic inside unit circle, and are expressed by Laurent series,

$$\phi_2(\zeta) = \phi_{21}(\zeta) + \phi_{22}(\zeta), \quad \psi_2(\zeta) = \psi_{21}(\zeta) + \psi_{22}(\zeta), \tag{A.2}$$

where

$$\phi_{21}(\zeta) = c_0 + c_1\zeta + c_2\zeta^2 + \cdots, \quad \phi_{22}(\zeta) = c_{-1}\frac{1}{\zeta} + c_{-2}\frac{1}{\zeta^2} + \cdots,$$

$$\psi_{21}(\zeta) = d_0 + d_1\zeta + d_2\zeta^2 + \cdots, \quad \psi_{22}(\zeta) = d_{-1}\frac{1}{\zeta} + d_{-2}\frac{1}{\zeta^2} + \cdots. \tag{A.3}$$

The following relations hold because of the mapping,

$$\phi_{21}\left(\frac{m}{\zeta}\right) - \phi_{21}(0) = \phi_{22}(\zeta),$$

$$\psi_{21}\left(\frac{m}{\zeta}\right) - \psi_{21}(0) = \psi_{22}(\zeta). \tag{A.4}$$

Taking the integrations, $(1/2\pi i)\int_\gamma 1/(\tau-\zeta)\,d\tau$, where $|\zeta| > 1$ and γ denotes the unit circle $|\zeta| = 1$, on (6), we obtain

$$-\phi_1(\zeta) + \phi_{22}(\zeta) + \frac{\zeta^2+m}{\zeta(1-m\zeta^2)}\bar{\phi}'_{21}\left(\frac{1}{\zeta}\right) + \frac{1+m^2}{2m}\frac{1}{\zeta - \frac{1}{\sqrt{m}}}\bar{\phi}'_{21}(\sqrt{m}) + \frac{1+m^2}{2m}\frac{1}{\zeta + \frac{1}{\sqrt{m}}}\bar{\phi}'_{21}(-\sqrt{m}) + \bar{\psi}_{21}\left(\frac{1}{\zeta}\right) - \bar{\psi}_{21}(0) = g_1(\zeta),$$

$$-\frac{\kappa_1}{2\mu_1}\phi_1(\zeta) + \frac{\kappa_2}{2\mu_2}\phi_{22}(\zeta) - \frac{1}{2\mu_2}\frac{\zeta^2+m}{\zeta(1-m\zeta^2)}\bar{\phi}'_{21}\left(\frac{1}{\zeta}\right) - \frac{1}{2\mu_2}\frac{1+m^2}{2m}\frac{1}{\zeta - \frac{1}{\sqrt{m}}}\bar{\phi}'_{21}(\sqrt{m}) - \frac{1}{2\mu_2}\frac{1+m^2}{2m}\frac{1}{\zeta + \frac{1}{\sqrt{m}}}\bar{\phi}'_{21}(-\sqrt{m}) - \frac{1}{2\mu_2}\bar{\psi}_{21}\left(\frac{1}{\zeta}\right) + \frac{1}{2\mu_2}\bar{\psi}_{21}(0) = 0, \tag{A.5}$$

where

$$g_1(\zeta) = \frac{1}{2\pi i}\int_\gamma \frac{g(\tau)}{\tau - \zeta}d\tau. \tag{A.6}$$

The same integrations on the conjugates of the two equations in (6) give

$$-\frac{\zeta(1+m\zeta^2)}{\zeta^2-m}\phi'_1(\zeta) - \psi_1(\zeta) + \bar{\phi}_{21}\left(\frac{1}{\zeta}\right) - \bar{\phi}_{21}(0) + \frac{1+m^2}{2}\left[\frac{1}{\zeta - \sqrt{m}}\phi'_{21}(\sqrt{m}) + \frac{1}{\zeta + \sqrt{m}}\phi'_{21}(\sqrt{-m})\right] + \frac{\zeta(1+m\zeta^2)}{\zeta^2-m}\phi'_{22}(\zeta) + \psi_{22}(\zeta) = g_2(\zeta),$$

$$\frac{1}{2\mu_1}\frac{\zeta(1+m\zeta^2)}{\zeta^2-m}\phi_1'(\zeta)+\frac{1}{2\mu_1}\psi_1(\zeta)+\frac{\kappa_2}{2\mu_2}\bar{\phi}_{21}\left(\frac{1}{\zeta}\right)-\frac{\kappa_2}{2\mu_2}\bar{\phi}_{21}(0)$$

$$-\frac{1}{2\mu_2}\frac{1+m^2}{2}\left[\frac{1}{\zeta-\sqrt{m}}\phi_{21}'(\sqrt{m})+\frac{1}{\zeta+\sqrt{m}}\phi_{21}'(\sqrt{-m})\right]-\frac{1}{2\mu_2}\frac{\zeta(1+m\zeta^2)}{\zeta^2-m}\phi_{22}'(\zeta)-\frac{1}{2\mu_2}\psi_{22}(\zeta)=0, \quad \text{(A.7)}$$

where

$$g_2(\zeta)=\frac{1}{2\pi i}\int_\gamma\frac{\overline{g(\tau)}}{\tau-\zeta}d\tau. \quad \text{(A.8)}$$

The following equation is obtained by (A.5.1) − (A.5.2) × $2\mu_1/\kappa_1$,

$$\frac{\mu_2\kappa_1-\mu_1\kappa_2}{\mu_2\kappa_1+\mu_1}\bar{\phi}_{22}(\zeta)+\frac{1+m^2}{2m}\left[\frac{1}{\zeta-\frac{1}{\sqrt{m}}}\phi_{21}'(\sqrt{m})+\frac{1}{\zeta+\frac{1}{\sqrt{m}}}\phi_{21}'(\sqrt{-m})\right]$$

$$-\frac{m\zeta(\zeta^2+m)}{1-m\zeta^2}\phi_{22}'(m\zeta)+\psi_{22}(m\zeta)=\frac{\mu_2\kappa_1}{\mu_2\kappa_1+\mu_1}\overline{g_1}(\zeta). \quad \text{(A.9)}$$

Similarly, (A.7.1) + (A.7.2) × $2\mu_1$ gives

$$\frac{\mu_1\kappa_2+\mu_2}{\mu_2-\mu_1}\bar{\phi}_{22}(m^2\zeta)+\frac{1+m^2}{2m}\left[\frac{1}{\zeta-\frac{1}{\sqrt{m}}}\phi_{21}'(\sqrt{m})+\frac{1}{\zeta+\frac{1}{\sqrt{m}}}\phi_{21}'(\sqrt{-m})\right]$$

$$+\frac{\zeta(1+m^3\zeta^2)}{m\zeta^2-1}\phi_{22}'(m\zeta)+\psi_{22}(m\zeta)=\frac{\mu_2}{\mu_2-\mu_1}g_2(m\zeta). \quad \text{(A.10)}$$

In obtaining (A.9) and (A.10), we have made use of (A.4). Also, we have replaced the variable ζ by $m\zeta$ in (A.10). By (A.9) − (A.10), an ordinary differential equation for $\phi_{22}(\zeta)$ is obtained,

$$\frac{\mu_1\kappa_2+\mu_2}{\mu_2-\mu_1}\bar{\phi}_{22}(\zeta)+\frac{\mu_1\kappa_2-\mu_2\kappa_1}{\mu_2\kappa_1+\mu_1}\bar{\phi}_{22}\left(\frac{\zeta}{m^2}\right)-(1-m^2)\frac{\zeta}{m^2}\phi_{22}'\left(\frac{\zeta}{m}\right)=q(\zeta), \quad \text{(A.11)}$$

where

$$q(\zeta)=-\frac{\mu_2\kappa_1}{\mu_2\kappa_1+\mu_1}\overline{g_1}\left(\frac{\zeta}{m^2}\right)+\frac{\mu_2}{\mu_2-\mu_1}g_2\left(\frac{\zeta}{m}\right). \quad \text{(A.12)}$$

Using (7), we evaluate the integrals in (A.6) and (A.8) to obtain

$$q(\zeta)=\frac{-\kappa_1\mu_2}{\kappa_1\mu_2+\mu_1}\frac{C}{2\pi i}\left(-2-\frac{\pi i m^2}{\zeta}+\frac{\zeta^2-m^4}{m^2\zeta}\log\frac{\zeta+m^2}{\zeta-m^2}\right)$$

$$+\frac{\mu_2}{\mu_2-\mu_1}\frac{C}{2\pi i}\left(-2+\frac{\pi i m}{\zeta}+\frac{\zeta^2-m^2}{m\zeta}\log\frac{\zeta+m}{\zeta-m}\right). \quad \text{(A.13)}$$

Generally, the solution for $\phi_{22}(\zeta)$ in (A.11) is expressed in terms of series. We write

$$q(\zeta)=\sum_{n=1}^{\infty}f_n\frac{1}{\zeta^n},$$

$$\phi_{22}(\zeta)=\sum_{n=1}^{\infty}a_n\frac{1}{\zeta^n}, \quad \text{(A.14)}$$

where f_n $(n=1,2,\ldots)$ are the known coefficients from the series expansion of (A.13). We obtain $\phi_{22}(\zeta)$ by substituting (A.14) into (A.11) and comparing the coefficients of both sides.

By (A.5.1) + (A.5.2) × $2\mu_2$, the potential $\phi_1(\zeta)$ is obtained as

$$\phi_1(\zeta)=-\frac{\mu_1}{\mu_2\kappa_1+\mu_1}g_1(\zeta)+\frac{\mu_1(1+\kappa_2)}{\mu_2\kappa_1+\mu_1}\phi_{22}(\zeta). \quad \text{(A.15)}$$

Similarly, (A.7.1) + (A.7.2) × $2\mu_2$ gives

$$\psi_1(\zeta) = -\frac{\mu_1}{\mu_1-\mu_2}g_2(\zeta) - \zeta\frac{1+m\zeta^2}{\zeta^2-m}\phi_1'(\zeta) + \frac{\mu_1(1+\kappa_2)}{\mu_1-\mu_2}\bar{\phi}_{22}(m\zeta). \tag{A.16}$$

Evaluating the integrals in (A.15) and (A.16), we have the final result,

$$\phi_1(\zeta) = \frac{1}{\Gamma\kappa_1+1}\frac{C}{2\pi i}\left[-2+\frac{i\pi}{\zeta}+\frac{\zeta^2-1}{\zeta}\log\frac{\zeta+1}{\zeta-1}\right] + \frac{1+\kappa_2}{\Gamma\kappa_1+1}\frac{C}{2}\frac{(P_3m+P_4)m}{P_1+P_2m^2+1-m^2}\frac{1}{\zeta} - \frac{1+\kappa_2}{\Gamma\kappa_1+1}\frac{2C}{\pi i}\sum_{n=1}^{\infty}a_{2n}m^{2n}\frac{1}{\zeta^{2n}},$$

$$\psi_1(\zeta) = \frac{1}{\Gamma-1}\frac{C}{2\pi i}\left[-2+\frac{i\pi}{\zeta}+\frac{\zeta^2-1}{\zeta}\log\frac{\zeta+1}{\zeta-1}\right]$$

$$-\frac{\zeta+m\zeta^3}{\zeta^2-m}\phi_1'(\zeta) + \frac{1+\kappa_2}{1-\Gamma}\frac{C}{2}\frac{(P_3m+P_4)}{P_1+P_2m^2+1-m^2}\frac{1}{\zeta} + \frac{1+\kappa_2}{1-\Gamma}\frac{2C}{\pi i}\sum_{n=1}^{\infty}a_{2n}\frac{1}{\zeta^{2n}}, \tag{A.17}$$

where $\Gamma = \mu_2/\mu_1$ and

$$a_{2n} = \frac{2(1-m^2)nm^{2n-1}+(P_1+P_2m^{4n})}{(P_1+P_2m^{4n})^2-4n^2(1-m^2)^2m^{4n-2}}(P_3m^{2n}-P_4)\frac{1}{4n^2-1},$$

$$P_1 = \frac{\Gamma+\kappa_2}{\Gamma-1}, \quad P_2 = -\frac{\Gamma\kappa_1-\kappa_2}{\Gamma\kappa_1+1},$$

$$P_3 = \frac{\Gamma\kappa_1}{\Gamma\kappa_1+1}, \quad P_4 = \frac{\Gamma}{\Gamma-1}. \tag{A.18}$$

The two potentials for the inclusion, $\phi_2(\zeta)$ and $\psi_2(\zeta)$, can also be obtained.